

Simple ROI Cone–Beam Computed Tomography

Michael Knaup, Clemens Maaß, Stefan Sawall, and Marc Kachelrieß

Abstract—High spatial resolution and large field of measurement are often contradictory demands, especially in x–ray cone–beam CT. On the one hand the number of detector elements are limited to typically 1024×1024 to 4096×4096 . On the other hand CT requires to completely cover the lateral field of measurement (FOM) with the detector. If the number of detector elements in the lateral direction is called M and the diameter of the field of measurement is D the spatial resolution that can be achieved is in the order of D/M .

Zooming into an object by a factor of 10, say, which can be done by decreasing the distance of the focal spot to the isocenter by the same factor, however yields truncated projections. We developed and implemented three methods that use a priori information from a low resolution overview scan to compensate for the data missing in the high resolution scan. These are the data completion, the data filtering, and the data weighting method. Thereby we were aiming at a robust and efficient solution with high image quality and high computational performance.

I. INTRODUCTION

AIMING at high spatial resolution in objects with a large transversal diameter requires to challenge the problem of transversal data truncation. For example the specific case we are interested in are objects fitting into a $D_L = 60$ mm diameter field of measurement (FOM) that shall be scanned with a circular cone–beam CT scanner whose flat detector consists of 2000×2000 elements. A standard scan would allow us to achieve a spatial resolution of roughly $30 \mu\text{m}$ assuming the focal spot size to be small enough. However, we are aiming at high–resolution imaging a $D_H = 6$ mm diameter region of interest, the ROI, with roughly $3 \mu\text{m}$ spatial resolution. To zoom into the object and increase the scanner’s magnification by a factor of 10 the distance of the focal spot to the isocenter can be reduced by the same factor, for example. The projection data p_H of this high resolution scan are, however, truncated in the lateral direction. To compensate for the information missing in the high resolution scan we use the projection data p_L of the standard or overview scan, which we will refer to as the low resolution scan in the following.

For some objects or scanner geometries, and for large zoom factors, it may happen that the x–ray source or the detector would collide with the object during the high resolution circle scan. To workaround this problem one could use object–dependent non–circular trajectories, as we did propose in reference [1] several years ago. Due to practical reasons and due to the scanner design constraints we are, however, restricted to certain scan trajectories (in our case circle scans or spiral scans). To avoid collision we can neither acquire a full 360° data set nor even a 180° data set, in general. Hence

Dr. Michael Knaup, Clemens Maaß, Stefan Sawall, Prof. Dr. Marc Kachelrieß: Institute of Medical Physics (IMP), University of Erlangen–Nürnberg, Henkestr. 91, 91052 Erlangen, Germany.

Corresponding author: marc.kachelrieß@imp.uni-erlangen.de



Fig. 1. State-of-the-art dimensional CT scanner used for our studies. The scanner is capable of CT rasterization and of ROI tomography. It acquires in circular and spiral mode.

it may happen that the high resolution scan is a limited angle scan that further suffers from lateral data truncation.

The literature describes several methods to do region-of-interest CT, which means to perform reconstruction from truncated data. All methods deal with the truncation problem and do not allow for a limited angle high resolution scan.

All practical solutions described make use of the low resolution data p_L to complete the data missing in p_H . This is either done in the rawdata domain itself, e.g. by rebinning, or it is done by reconstructing the low resolution data to obtain a low resolution volume f_L which then can be forward projected using the geometry of the high resolution scan to provide rawdata that completes p_H [2], [3], [4], [5], [6], [7].

Further on, there are numerous methods that seek reconstructing from the high resolution data only without having low resolution overview scans available. Those are either of truncation–correction type with some kind of extrapolation designed for diagnostic purposes which yield less quantitative results [8], [9], [10], [11], [12], [13] or they are mathematical tweaks including some approximation or highly restrictive a priori assumptions [14], [15], [16]. A promising new interior tomography approach is based on compressed sensing which, however, requires long reconstruction times and the assumption of piecewise constant objects [17], [18], [19]. Due to these undesired properties these methods are considered to be impractical for our purposes and therefore not within the scope of this paper.

In principle, the first class of algorithms, that makes full use of the low resolution overview scan, provides adequate image quality for our purposes. However, one will run into

significant performance problems whenever the focal spot trajectory of the high resolution scan approaches the convex hull of the object. In this case the fan angle of the completed high resolution scan approaches 180° and a very large number of additional detector channels would be needed to complete the truncated region of the high resolution scan.

While one can certainly sidestep those issues, e.g. by using a virtual curved detector in place of a flat detector or by performing the forward projections on a sparse grid instead of using the high resolution grid, we propose two simple rawdata-based methods that require reconstructions of p_L but that do not require forward projections at all. It should be noted that our methods can easily be combined with the possibility of laterally shifting the detector to increase the object coverage or the spatial resolution by another factor of two [20], [21], [22], [23]. In this study, however, we did not make use of this option and only deal with data from non-shifted detectors.

II. MATERIALS AND METHODS

We discuss the reconstruction of cone-beam CT data of the form

$$p(\alpha, \vartheta, \gamma) = \int_0^\infty d\lambda f(\mathbf{s} + \lambda\Theta)$$

with $\mathbf{s} = \mathbf{s}(\alpha)$ being the source position at time (or angle) α and

$$\Theta = \begin{pmatrix} -\sin \vartheta \cos \gamma \\ \cos \vartheta \cos \gamma \\ \sin \gamma \end{pmatrix}$$

being the direction vector of a ray emerging at $\mathbf{s}(\alpha)$ in the direction specified by the angles ϑ and γ . The rawdata are denoted as $p(\alpha, \vartheta, \gamma)$ and the object to be reconstructed is $f(\mathbf{r})$. Due to the limited detector size we will conduct two scans of the above type. One overview scan which covers the complete object and thereby results in low resolution data and one high resolution scan that covers only an ROI of the object. We use the subscripts L and H to distinguish between both scans.

Aiming at Feldkamp-type approximate image reconstruction we assume the source trajectory to approximately lie in a plane parallel to the x - y -plane and we assume the rotation axis to be parallel to the z -axis. Note that even if the scanner is performing exact circle scans the rotation axes of the low resolution overview scan and the high resolution scan do not necessarily coincide because the rotation center of the high resolution scan is determined by the position and size of the ROI.

Since we perform approximate and Feldkamp-type image reconstruction the angle γ of the ray is used for length correction only. It does not play a role in the data consistency and weighting criteria discussed below. Therefore we may safely drop γ in the following and restrict ourselves to in-plane considerations, i.e. to the two dimensions x and y .

To achieve data consistency and to define appropriate weighting functions it is necessary to parameterize a ray by its angle ϑ and its distance ξ with respect to the origin of the

coordinate system. While ϑ is already well defined we obtain ξ as a function of \mathbf{s} and ϑ as

$$\xi = \mathbf{s} \cdot \boldsymbol{\vartheta} = s_x \cos \vartheta + s_y \sin \vartheta$$

where we defined

$$\boldsymbol{\vartheta} = \begin{pmatrix} \cos \vartheta \\ \sin \vartheta \end{pmatrix}.$$

The ray specified by ϑ and ξ is the line

$$x \cos \vartheta + y \sin \vartheta = \xi.$$

Image reconstruction can be performed if the data are complete and if data redundancies are properly normalized by defining a weighting function $w(\vartheta, \xi)$ that is zero wherever rays are missing and that fulfills

$$\sum_k w(\vartheta + k\pi, (-)^k \xi) = 1, \quad (1)$$

as discussed in reference [23].

Although the methods presented work for general focal spot trajectories the CT scan modi we have in mind rather perform approximate circular scans. Restricting ourselves to such trajectories later allows us to formulate explicit equations for the weighting functions, which is more convenient for the reader. Therefore we introduce the circle trajectories

$$\mathbf{s}_L(\alpha) = \begin{pmatrix} R_{FL} \sin \alpha \\ -R_{FL} \cos \alpha \\ 0 \end{pmatrix} \text{ and } \mathbf{s}_H(\alpha) = \begin{pmatrix} R_{FH} \sin \alpha \\ -R_{FH} \cos \alpha \\ 0 \end{pmatrix} + \mathbf{o}$$

with R_F denoting the radii of the low and the high resolution scan trajectories, respectively, and with \mathbf{o} being the isocenter of the high resolution scan. We make use of these when defining the weight functions below.

In total we compare three different methods to perform ROI tomography when sufficient overview data are present: the data completion method which is in wide use already, the data filtering method, and the data weighting method. To our knowledge, the last two methods are new.

A. Data Completion Method

The classical data completion methods perform a forward projection of a low resolution overview volume f_L to complete data missing in the high resolution scan. While this is typically done to complete truncated data the same procedure could be used to solve the limited angle problem. As mentioned above the data completion may suffer from low performance and require a significant amount of memory.

To become more formal let us introduce some notation. Let X_L denote the x-ray transform corresponding to the overview scan and let $f_L = X_L^{-1} p_L$ be the said overview volume reconstructed from the measured low resolution data p_L . Let $X_H = X_M + X_U$ be a decomposition of the high resolution x-ray transform into rays that have been measured and those that are unmeasured. The high resolution projection data are denoted as p_H which we assume to be zero for all unmeasured rays, i.e. in the truncated region and in the regions where the projection angles are missing.

Using this notation the data completion method is given by the equation

$$f_H = X_H^{-1}(p_H + X_U f_L). \quad (2)$$

B. Data Filtering Method

Equation (2) is equivalent to

$$f_H = f_L + X_H^{-1}(p_H - X_M f_L)$$

because we have $f_L = X_H^{-1}(X_U f_L + X_M f_L)$ due to the linearity of the x-ray transform. The latter equation, however, has a different interpretation. It implies that the rawdata obtained by forward projection of the overview scan are subtracted from the measured high resolution rawdata in the measured region(s), and that those rawdata are reconstructed and added to the low resolution overview images.

While this sounds interesting a closer look at the subtraction term

$$p_H - X_M f_L$$

reveals that it is the difference between high resolution measured rawdata and low resolution virtual rawdata and thereby must be equivalent to a high-pass filtering of the measured data. If h denotes an appropriate high-pass filter then we may summarize our findings as

$$p_H - X_M f_L = h * p_H.$$

Hence, we can obtain the high resolution reconstruction as

$$f_H = f_L + X_H^{-1}(h * p_H) \quad (3)$$

which does not involve any forward projections.

To find the appropriate high-pass filter let us go to Fourier domain and let $MTF_L(u)$ and $MTF_H(u)$ be the presampling MTFs of the low resolution overview scan and of the high resolution ROI scan, respectively, both being scaled to the isocenter. Then, the high-pass filter $H(u)$ should have the property

$$MTF_L(u) + MTF_H(u)H(u) = MTF_H(u).$$

Solving for $H(u)$ yields

$$H(u) = 1 - \frac{MTF_L(u)}{MTF_H(u)}.$$

Note that the simplicity of the data filtering method is appealing. Although the method is analytically equivalent to the completion method this is not true numerically. The downside of the data filtering method is increased image noise and increased susceptibility to artifacts in the high resolution region since the method just adds a correction term to the low resolution data and thereby cannot eliminate image noise or artifacts inherent in f_L .

C. Data Weighting Method

Our third method has two advantages: the advantage of the data completion method of not having artifacts propagating into the high resolution ROI and the advantage of the high-pass filtering method of being computationally highly efficient. This is achieved by designing appropriate weighting functions $w_L(\vartheta, \xi)$ and $w_H(\vartheta, \xi)$ that shall be multiplied to the low and high resolution rawdata, respectively.

To start, let us define a redundancy weight $w_R(\vartheta, \xi)$. Whenever the scan range exceeds 180° plus fan angle we need to

either weight the data with a short scan weight, which is also known as the Parker weight function, or if the scan exceeds 360° we need to weight the data with the overscan weight function. In case of a shifted detector design the corresponding shifted detector weight can be applied. These redundancy weight functions can be taken from reference [23], for example. Since the focal spot trajectory of the low resolution and of the high resolution scan differ, in general, we need to use two different redundancy weight functions $w_{RL}(\vartheta, \xi)$ and $w_{RH}(\vartheta, \xi)$, respectively. The redundancy weights fulfill equation (1) as shown in reference [23].

In addition a weight function $w_M(\vartheta, \xi)$ is needed whose support corresponds to the measured high resolution data. This means that w_M is zero wherever the high resolution scan has missing rays and it smoothly increases to one where measured high resolution data are available. Hence w_M masks out the truncated regions of the detector and the unmeasured angular positions.

We now set

$$\begin{aligned} w_H(\vartheta, \xi) &= w_{RH}(\vartheta, \xi)w_M(\vartheta, \xi) \\ w_L(\vartheta, \xi) &= w_{RL}(\vartheta, \xi)\left(1 - \sum_k w_H(\vartheta + k\pi, (-)^k \xi)\right). \end{aligned}$$

Then

$$f_H = X_L^{-1}p_L w_L + X_H^{-1}p_H w_H \quad (4)$$

yields the final volume in the high resolution ROI.

To see that everything is properly normalized let us temporarily abbreviate $w(\vartheta + k\pi, (-)^k \xi)$ as $w(k)$. Keeping in mind that w_{RL} is properly normalized, because $\sum_k w_{RL}(k) = 1$ by definition, we are now ready to check whether $w_L + w_H$ is properly normalized. We find

$$\begin{aligned} \sum_k (w_L(k) + w_H(k)) &= \\ \sum_k (w_{RL}(k)(1 - \sum_l w_H(k+l)) + w_H(k)) &= \\ \sum_k w_{RL}(k)(1 - \sum_l w_H(k+l)) + \sum_k w_H(k) &= \\ \sum_k w_{RL}(k)(1 - \sum_l w_H(l)) + \sum_l w_H(l) &= \\ \sum_k w_{RL}(k) + \sum_l w_H(l)(1 - \sum_k w_{RL}(k)) &= 1. \end{aligned}$$

To conclude this section, let us give an example of how to define the weight function $w_M(\vartheta, \xi)$ that is smooth and masks out the unmeasured regions for the simple case of scanning a cylindrical high resolution ROI of radius R_{MH} and center \mathbf{o} . Note that a ray through the center of the ROI has the lateral coordinate $\xi_C = \mathbf{o} \cdot \vartheta$ which is a function of the angle ϑ , in general.

Let $s(x)$ have the properties $s(-x) = -s(x)$ and $s(1) = 1$. Given that we apply the data weighting method to sampled data it is also recommended to choose s to be smooth. We use $s(x) = \sin(\frac{1}{2}\pi x)$ for our numerical experiments. Now we can define the mask function which in this case is a simple

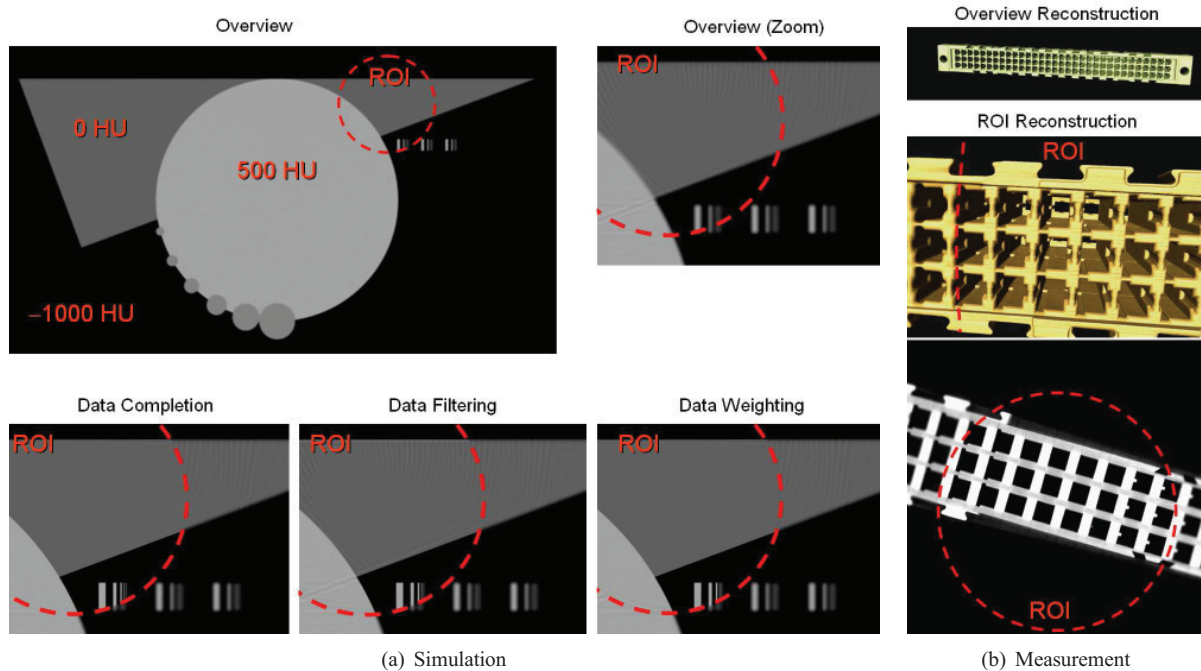


Fig. 2. a) The simulated test phantom is shown in a low resolution overview reconstruction, a low resolution zoom version where the FOV corresponds to the FOV used for the high resolution reconstructions. The high resolution reconstructions (bottom row) indicate that all three methods, the data completion, the high-pass filtering and the data weighting method achieve equivalent results. b) Reconstructions of a measured connector element showing a low resolution overview volume rendering, and a high resolution ROI reconstruction using the data weighting method. The high resolution volume is shown as a volume rendering and as a CT slice. Within the ROI the desired high spatial resolution is achieved.

radial transition weight function

$$w_M(\vartheta, \xi) = \frac{1}{2} \begin{cases} 0 & \text{if } \xi < \xi_A \\ 1 + s \left(2 \frac{\xi - \xi_A}{\xi_B - \xi_A} - 1 \right) & \text{else if } \xi < \xi_B \\ 2 & \text{else if } \xi < \xi_D \\ 1 - s \left(2 \frac{\xi - \xi_D}{\xi_E - \xi_D} - 1 \right) & \text{else if } \xi < \xi_E \\ 0 & \text{else} \end{cases}$$

that is zero in the outer region and smoothly increases to one in the inner region of the high resolution scan. The parameters $\xi_A < \xi_B < \xi_C < \xi_D < \xi_E$ are functions of ϑ and specify the lateral detector limits of the high resolution scan, and the transition regions where the weight smoothly increases from zero to one, and the center of the detector, as discussed above. With $\xi_C = \mathbf{o} \cdot \boldsymbol{\vartheta}$ we use $\xi_A = \xi_C - R_{MH}$, $\xi_B = \xi_C - R_{MH} + \Delta R$, $\xi_D = \xi_C + R_{MH} - \Delta R$, and $\xi_E = \xi_C + R_{MH}$ with ΔR being the size of the transition zone, $0 < \Delta R \ll R_{MH}$.

III. EXPERIMENTS

To evaluate the three methods defined in equations (2), (3) and (4) we conducted several simulations and measurements. The simulations were carried out by the analytical projection simulator RayConStruct PS (RayConStruct GmbH, Nürnberg, Germany). The measurements were done using the TomoScope HV 500 cone-beam CT scanner (Werth Messtechnik GmbH, Gießen, Germany). The tube voltage was 200 kV.

The geometry is a flat detector cone-beam geometry with about 1000 projections per full rotation and a detector with about 1000 by 1000 detector pixels of size 0.4 mm. The

distance of the focal spot to the detector surface was chosen as 2400 mm and the radii of the circle scans were set to $R_{FL} = 1200$ mm and $R_{FH} = 150$ mm for the low resolution overview and the high resolution ROI scan, respectively. This results in a radius of the field of measurement of $R_{ML} = 100$ mm for the overview scan and of $R_{MH} = 12.5$ mm for the ROI scan. Thus, the ROI scan zooms into the object by a factor of eight.

IV. RESULTS

Figure 2a) shows various reconstructions of the simulated test phantom. The overview image depicts all objects within the low resolution field of measurement. A dashed circle indicates the region of interest. There is also a zoom version of the overview image which was produced by reconstructing the overview data p_L on the same voxel grid as will be used for the reconstructions of the ROI data. The three images at the bottom row of subfigure a) are the ROI reconstructions that use the three methods data completion, data filtering and data weighting to combine p_L with p_H .

The measured connector element is presented in figure 2b). The overview scan p_L can be used to reconstruct the complete object (here, a volume rendering of the connector is shown). The ROI reconstructions (one volume rendering and one transversal slice) instead only show a portion of the connector with high spatial resolution within the cylindrical ROI and low spatial resolution outside the ROI. Due to space limitations the measurement is only shown using the data weighting method.

Figure 3 is the scan of a chromatography column. Only a square section centered around the ROI is shown in four

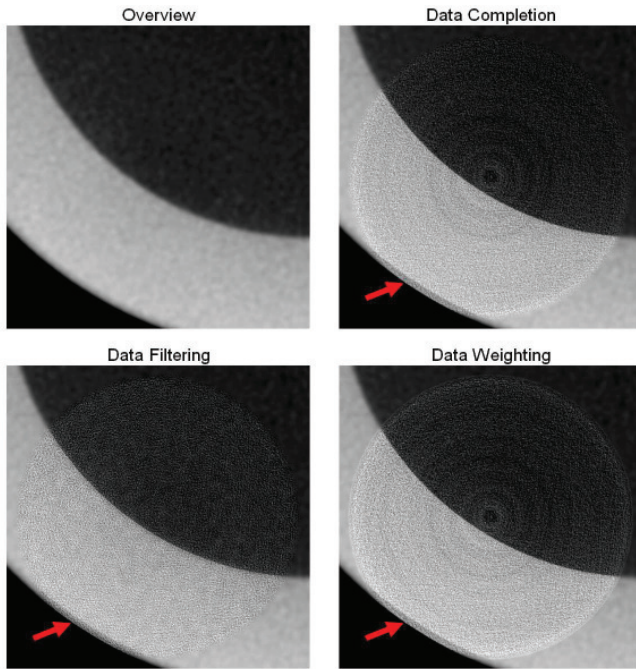


Fig. 3. Chromatography column filled with silica gel. The figures show the zoomed FOV of the ROI. The 50 mm inner diameter is surrounded by a 9 mm thick glass cylinder which is surrounded by a 0.5 mm splinter shield (scatter protection) foil. Only the ROI reconstructions show the scatter protection foil (arrows). The ROI diameter is 25 mm.

versions: overview image, data completion method, data filtering method, and data weighting method. The properties of the filtering method are as expected because noise is increased. Rather unexpected but quite evident is the fact that the only ROI method that does not show ring artifacts is the data filtering method while the completion and the weighting methods show some ring artifacts.

V. DISCUSSION

Whenever an overview scan is available it is relatively simple to perform local tomography. To improve the computational performance and to reduce the memory requirements we proposed two methods that do not need to complete the truncated data of the high resolution scan and that do not need to perform forward projections of an overview volume. In fact these two methods do not even need to reconstruct the overview volume. While our preliminary results shown here give the impression that the data filtering method is of equal image quality as the data weighting method a further analysis using simulations and measurements shows that this is not always the case. Noise and artifacts that propagate from the low resolution reconstruction into the ROI cannot be removed by the data filtering method. The data weighting method, however, does not suffer from those artifacts because only very low frequencies propagate from the low resolution data into the high resolution scan.

Summarizing, we evaluated three highly promising approaches that are readily applicable for industrial tomography.

ACKNOWLEDGMENTS

This work was supported in parts by the AiF under grant KF2336201FO9. The scans were carried out by Werth Messtechnik GmbH, Gießen, Germany. The chromatography column was provided by the Lehrstuhl für Thermische Verfahrenstechnik, University of Erlangen–Nürnberg, Germany. Parts of the reconstruction software were provided by RayConstruct GmbH, Nürnberg, Germany. We thank the Intel Corporation and Fujitsu Siemens Computers GmbH for providing the highly performant compute hardware.

REFERENCES

- [1] C. Penßel, W. A. Kalender, and M. Kachelrieß, "ROI-driven CT trajectories," *IEEE Medical Imaging Conference Record*, pp. M06–181, 1969–1972, 2006.
- [2] D. Gentle and N. Spyrou, "Region of interest tomography in industrial applications," *Nuclear Instruments and Methods in Physics Research*, vol. A299, pp. 534–537, 1990.
- [3] S. Azevedo, P. Rizo, and P. Grangeat, "Region-of-interest cone-beam computed tomography," Lawrence Livermore National Lab., CA (United States), Tech. Rep., June 1995.
- [4] I. K. Chun, M. H. Cho, S. C. Lee, M. H. Cho, and S. Y. Lee, "X-ray micro-tomography for small-animal imaging with zoom-in imaging capability," *Phys. Med. Biol.*, vol. 49, pp. 3889–3902, 2004.
- [5] J. Wiegert, M. Bertram, T. Netsch, J. Wulff, J. Weese, and G. Rose, "Projection extension for region of interest imaging in cone-beam CT," *Academic Radiology*, vol. 12, pp. 1010–1023, 2005.
- [6] S. Y. Lee, M. H. Cho, S. C. Lee, I. K. Chun, and J. J. Park, "Small animal x-ray micro-CT with zoom-in imaging capability," *IEEE Medical Imaging Conference Record*, pp. M14–156, 3102–3105, 2006.
- [7] L. Chen, Y. Shen, C.-J. Lai, T. Han, Y. Zhong, S. Ge, X. Liu, T. Wang, W. T. Yang, G. J. Whitman, and C. C. Shaw, "Dual resolution cone beam breast CT: A feasibility study," *Med. Phys.*, vol. 36, no. 9, pp. 4007–4914, Sep. 2009.
- [8] R. Lewitt, "Processing of incomplete measurement data in computed tomography," *Med. Phys.*, vol. 6, no. 5, pp. 412–417, 1979.
- [9] D. Kadrmas, R. Jaszczak, J. McCormick, R. Coleman, and C. Lim, "Truncation artifact reduction in transmission CT for improved SPECT attenuation compensation," *Phys. Med. Biol.*, vol. 40, pp. 1085–1104, 1995.
- [10] B. Ohnesorge, T. Flohr, K. Schwarz, J. Heiken, and K. Bae, "Efficient correction for CT image artifacts caused by objects extending outside the scan field of view," *Med. Phys.*, vol. 27, no. 1, pp. 39–46, Jan. 2000.
- [11] J. Hsieh, E. Chao, J. Thibault, B. Grekowitz, A. Horst, S. McOlash, and T. Myers, "Algorithm to extend reconstruction field-of-view," *IEEE International Symposium on Biomedical Imaging*, pp. 1404–1407, Apr. 2004.
- [12] C. Penßel, M. Kachelrieß, and W. A. Kalender, "Hybrid detruncation HDT algorithm for the reconstruction of CT data," *Radiology*, vol. 233(P), p. 293, Nov. 2004.
- [13] K. Sourbelle, M. Kachelrieß, and W. A. Kalender, "Reconstruction from truncated projections in CT using adaptive detruncation," *European Radiology*, vol. 15, no. 5, pp. 1008–1014, May 2005.
- [14] X. Pan, Y. Zou, and D. Xia, "Peripheral and central ROI-image reconstruction from and data-redundancy exploitation in truncated fan-beam data," *Med. Phys.*, vol. 32, no. 3, pp. 673–684, Mar. 2005.
- [15] M. Courdurier, F. Noo, M. Defrise, and H. Kudo, "Solving the interior problem of computed tomography using a priori knowledge," *Inverse Problems*, vol. 24, p. 065001, 2008.
- [16] H. Kudo, M. Courdurier, F. Noo, and M. Defrise, "Tiny a priori knowledge solves the interior problem in computed tomography," *Phys. Med. Biol.*, vol. 53, pp. 2207–2231, 2008.
- [17] X. Pan, E. Sidky, and M. Vannier, "Why do commercial CT scanners still employ traditional, filtered back-projection for image reconstruction?" *Inverse Problems*, vol. 25, no. 12, pp. 1–36, Dec. 2009.
- [18] H. Yu and G. Wang, "Compressed sensing based interior tomography," *Phys. Med. Biol.*, vol. 54, pp. 2791–2805, 2009.
- [19] H. Yu, J. Yang, M. Jiang, and G. Wang, "Supplemental analysis on compressed sensing based interior tomography," *Phys. Med. Biol.*, vol. 54, pp. N425–N432, 2009.

- [20] P. S. Cho, A. D. Rudd, and R. H. Johnson, "Cone-beam CT from width-truncated projections," *Computerized Medical Imaging and Graphics*, vol. 20, no. 1, pp. 49–57, 1996.
- [21] G. Wang, "X-ray micro-CT with a displaced detector array," *Med. Phys.*, vol. 29, no. 7, pp. 1634–1636, Jul. 2002.
- [22] V. Liu, N. R. Lariviere, and G. Wang, "X-ray micro-CT with a displaced detector array: Application to helical cone-beam reconstruction," *Med. Phys.*, vol. 30, no. 10, pp. 2758–2761, Oct. 2003.
- [23] C. Maaß, M. Knaup, R. Lapp, M. Karolczak, W. A. Kalender, and M. Kachelrieß, "A new weighting function to achieve high temporal resolution in circular cone-beam CT with shifted detectors," *Med. Phys.*, vol. 35, no. 12, pp. 5898–5909, Dec. 2008.